Bioactive Materials 40 (2024) 634–648

Contents lists available at ScienceDirect

Bioactive Materials

journal homepage: www.keaipublishing.com/en/journals/bioactive-materials

A novel mesenchymal stem cell-targeting dual-miRNA delivery system based on aptamer-functionalized tetrahedral framework nucleic acids: Application to endogenous regeneration of articular cartilage

Liwei Fu [a,b,c,d,1], Jiang Wu [b,c,d,f,1], Pinxue Li [a,b,1], Yazhe Zheng [b,c,d,f], Zhichao Zhang [a,b,c,d], Xun Yuan [b,c,d,f], Zhengang Ding [b,c,d,f], Chao Ning [b,c,d], Xiang Sui [b,c,d], Shuyun Liu [a,b,c,d,****], Sirong Shi [e,***], Quanyi Guo [a,b,c,d,**], Yunfeng Lin [e,*]

[a] School of Medicine, Nankai University, Tianjin, 300071, People's Republic of China
[b] Institute of Orthopedics, The First Medical Center, Chinese PLA General Hospital, Beijing Key Lab of Regenerative Medicine in Orthopedics, Key Laboratory of Musculoskeletal Trauma & War Injuries PLA, No. 28 Fuxing Road, Haidian District, Beijing, People's Republic of China
[c] Department of Orthopedics, The Fourth Medical Center, Chinese PLA General Hospital, Beijing, People's Republic of China
[d] National Clinical Research Center for Orthopedics, Sports Medicine & Rehabilitation, Beijing, People's Republic of China
[e] State Key Laboratory of Oral Diseases, National Clinical Research Center for Oral Diseases, West China Hospital of Stomatology, Sichuan University, Chengdu, 610041, People's Republic of China
[f] Guizhou Medical University, Guiyang, 550004, Guizhou Province, People's Republic of China

ARTICLE INFO

Keywords:
Tetrahedral framework nucleic acids
miRNAs co-delivery
Targeting system
Articular cartilage endogenous regeneration
Mesenchymal stem cells

ABSTRACT

Articular cartilage injury (ACI) remains one of the key challenges in regenerative medicine, as current treatment strategies do not result in ideal regeneration of hyaline-like cartilage. Enhancing endogenous repair via microRNAs (miRNAs) shows promise as a regenerative therapy. miRNA-140 and miRNA-455 are two key and promising candidates for regulating the chondrogenic differentiation of mesenchymal stem cells (MSCs). In this study, we innovatively synthesized a multifunctional tetrahedral framework in which a nucleic acid (tFNA)-based targeting miRNA codelivery system, named A-T-M, was used. With tFNAs as vehicles, miR-140 and miR-455 were connected to and modified on tFNAs, while Apt19S (a DNA aptamer targeting MSCs) was directly integrated into the nanocomplex. The relevant results showed that A-T-M efficiently delivered miR-140 and miR-455 into MSCs and subsequently regulated MSC chondrogenic differentiation through corresponding mechanisms. Interestingly, a synergistic effect between miR-140 and miR-455 was revealed. Furthermore, A-T-M successfully enhanced the endogenous repair capacity of articular cartilage in vivo and effectively inhibited hypertrophic chondrocyte formation. A-T-M provides a new perspective and strategy for the regeneration of articular cartilage, showing strong clinical application value in the future treatment of ACI.

1. Introduction

The treatment of articular cartilage (AC) lesions induced by trauma, inflammation, or chronic strain represents a vital challenge for regenerative medicine and clinical needs [1,2]. Spontaneous regeneration of AC is considered unlikely due to its avascular status and nutrient deficiencies [3,4]. The current surgical treatment strategies for AC repair include microfracture techniques, autologous or allogeneic cartilage (cell) transplantation, and the implantation of cartilage scaffolds [1,5]. However, based on long-term follow-up results, these surgical strategies often result in the formation of fibrocartilage rather than durable functional hyaline cartilage [6–8]. In recent years, therapy

Peer review under responsibility of KeAi Communications Co., Ltd.
* Corresponding author.
** Corresponding author. School of Medicine, Nankai University, Tianjin, 300071, People's Republic of China.
*** Corresponding author.
**** Corresponding author. School of Medicine, Nankai University, Tianjin, 300071, People's Republic of China.
E-mail addresses: clear_ann@163.com (S. Liu), sirongshi@scu.edu.cn (S. Shi), doctorguo_301@163.com (Q. Guo), yunfenglin@scu.edu.cn (Y. Lin).
[1] These authors contributed equally to this work.

https://doi.org/10.1016/j.bioactmat.2024.08.008
Received 1 April 2024; Received in revised form 25 June 2024; Accepted 12 August 2024

based on mesenchymal stem cells (MSCs) has emerged as a frontier in development and has achieved encouraging results [9,10]. However, several potential issues, including the high cost of in vitro cultivation, loss of induced cell functionality and aging after cultivation, may limit the efficacy of in vitro-cultivated MSC therapy within the joint cavity [11,12].

Despite the relatively poor quality of regenerated tissue, the effectiveness of the microfracture technique suggests that the repair of AC injuries can be achieved by directly stimulating endogenous MSCs within the joint cavity [13,14]. Previous studies have confirmed the presence of MSCs at various sites within the joint, such as the bone marrow, infrapatellar fat pad, and synovium [15]. When AC is damaged, these resident intra-articular MSCs migrate and undergo chondrogenic differentiation at the site of the defect, which is referred to as endogenous repair [14,16]. Notably, osteotomy and knee joint distraction, commonly used for treatment of osteoarthritis, also rely on this endogenous repair capability [1]. Unfortunately, due to the disruption of the intra-articular microenvironment, the chondrogenic differentiation process of endogenous MSCs without intervention also gradually degenerates over time, eventually leading to a hypertrophic chondrocyte-like phenotype [2,17]. Therefore, the development of treatment strategies that can regulate the differentiation fate of endogenous MSCs and enhance their endogenous repair capacity is a highly promising clinical translational approach to address the issue of AC regeneration.

MicroRNAs (miRNAs) can regulate gene expression by interfering with mRNA translation and play an important role in cell fate [18,19]. Notably, miRNAs play a crucial role in cartilage development and homeostasis and are important regulators of the chondrogenesis of MSCs [20,21]. Among the miRNAs, miR-140 has been shown to be an essential upregulated factor induced by SOX9, with cartilage specificity, and to play a critical role in the MSC chondrogenic differentiation process [22–24]. Karlsen et al. demonstrated that miR-140 enhances the chondrogenic differentiation of human MSCs by targeting RALA [25]. Specifically, Zhao et al. reported that combined gene therapy with intra-articular administration of IGF-1 and miR-140 improved cartilage injury repair [26]. Furthermore, Rajagopal et al. reported that continuous delivery of miR-140 to MSCs in a three-dimensional (3D) matrix resulted in the formation of transparent cartilage-like tissue, reduced hypertrophy, and successfully simulated endogenous stem cell-mediated cartilage repair [27]. In addition, recent studies have revealed another key positive regulatory factor, miR-455, involved in the chondrogenic differentiation of MSCs [28,29]. Studies have shown that the expression of both miR-455–5p and miR-3p is upregulated by the overexpression of Sox9, which is highly expressed during the chondrogenic differentiation of MSCs [29]. In several published studies by Zhang et al., miR-455-3p was demonstrated to directly target Runx2 to activate early chondrogenesis and to inhibit the degenerative process of MSC chondrogenic differentiation through DNA methylation [29,30]. Moreover, Sun et al. confirmed that exosomes derived from TGF-β3-pretreated bone marrow MSCs promote AC regeneration by delivering miR-455 [31]. Overall, miR-140 and miR-455 are two promising candidates for regulating the differentiation of endogenous MSCs and enhancing the endogenous repair capacity of AC. We speculate that the codelivery of miR-140 and miR-455 may play a positive role in the repair and treatment of AC. However, due to their inherent limitations, such as poor stability, compatibility issues with commonly used delivery vectors, cell toxicity, and high off-target effects, miRNAs are substantially restricted in clinical applications. Therefore, there is an urgent need to develop a targeted codelivery system that can stably and efficiently deliver miR-140 and miR-455 to enhance the endogenous repair capacity of AC via miRNAs.

Tetrahedral framework nucleic acids (tFNAs), novel DNA nanomaterials with powerful biocompatibility, high editability, and cellular internalization capability, have emerged as ideal nanovehicles for drug delivery, demonstrating strong potential and value in the field of biomedicine [32,33]. In our early explorations, tFNAs demonstrated powerful regulatory effects on biological functions such as proliferation, migration, and differentiation of MSCs [34–36]. Furthermore, our previous studies have shown that tFNAs may be synergistic agents that promote the chondrogenic differentiation of synovium-derived MSCs (SMSCs) and enhance in situ AC regeneration in animal models [37]. Hence, tFNAs are ideal vehicles for the codelivery of miR-140 and miR-455 for the treatment of AC injury. In this work, we first synthesized a complex of tFNAs and miRNAs, referred to as tFNAs-miR140-miR455 (T-M). Then, we incorporated Apt19S [38,39], a DNA aptamer that specifically recognizes pluripotent stem cells, into T-M to establish a multifunctional tFNA-based miRNA delivery system, denoted “A-T-M”. We aimed for A-T-M to specifically codeliver miR-140 and miR-455 into MSCs to exert their roles in regulating cell differentiation. Additionally, we investigated the potential mechanisms of A-T-M through transcriptome sequencing and constructed a classic in vivo model of AC defects to explore the ability of A-T-M to enhance the endogenous repair capacity (Fig. 1). This work first reveals the synergistic effect of miR-140 and miR-455 on regulating MSC chondrogenic differentiation and represents a novel application of functional cartilage miRNAs combined with tFNAs. A-T-M indeed effectively enhances the endogenous repair of AC by regulating the chondrogenic differentiation of MSCs, indicating its potential as a regenerative enhancer for the treatment of AC defects with strong clinical application value in the future.

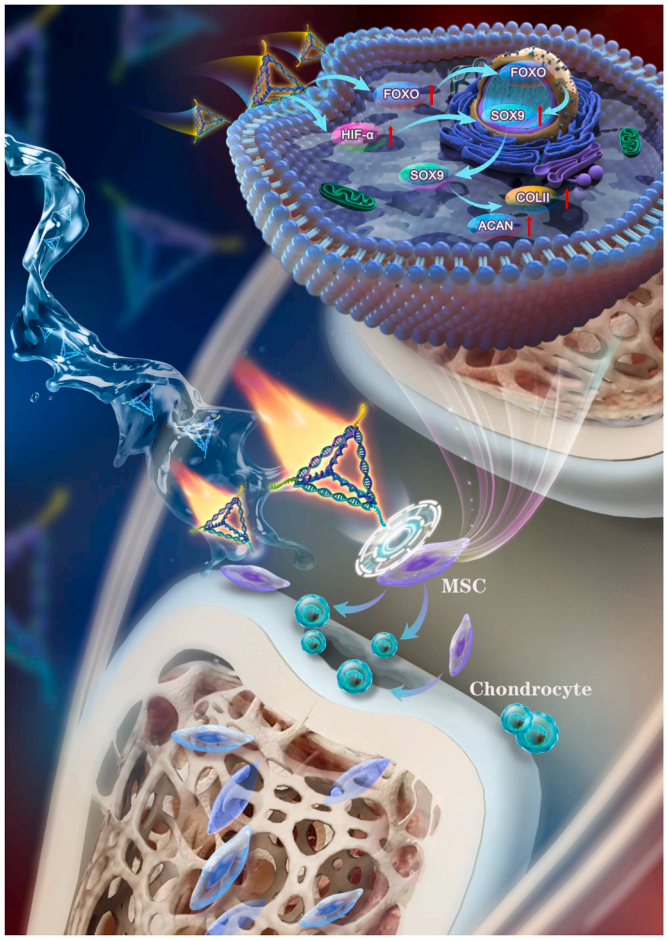

Fig. 1. A multifunctional tFNA-based miRNA delivery system enhances the endogenous repair of AC by modulating the chondrogenic differentiation of MSCs.

2. Results and discussion

2.1. Design, preparation, and characterization of A-T-M

As an ideal vehicle for miRNAs, tFNAs can be rapidly self-assembled from four predesigned ssDNA stands (S1, S2, S3 and S4; Table S1; Supporting Information) through a simple program [40], resulting in a strongly editable structure. However, the current methods for delivering miRNAs via tFNAs often lack specificity, and these molecules can be widely taken up by various types of cells, resulting in suboptimal therapeutic effects. Inspired by the precise targeting of missiles, we sought to develop a nanovehicle material based on the fundamental tFNA structure that can carry multiple miRNAs and target specific cells for delivery. In this study, miR-140-5p and miR-455-3p were added to the 3′ ends of S1 and S2, respectively, yielding S1-miR140 and S2-miR455 (Table S1, Supporting Information); subsequently, a DNA aptamer called Apt19S, which specifically recognizes pluripotent stem cells, was added to the 3′ end of S3 (S3-Apt19S; Table S1, Supporting Information). Finally, A-T-M was synthesized following the same steps as those used for tFNAs (Fig. 2A and Fig. S1A, Supporting Information).

According to the difference in mobility of these nanostructures, 8 % polyacrylamide gel electrophoresis (PAGE) was performed to confirm the successful synthesis of the tFNAs and A-T-M. The PAGE results (Fig. 2B) suggested that the mobility of A-T-M with a higher molecular weight was significantly slower than that of the tFNAs. Consistent with the PAGE results, the high-performance capillary electrophoresis (HPCE) results reconfirmed the successful synthesis of A-T-M (Fig. 2C and Fig. S2, Supporting Information). In addition, we performed dynamic light scattering (DLS) to determine the particle size and zeta potential of the tFNAs (Fig. S1B, Supporting Information) and A-T-M (Fig. 2D). The DLS results suggested that the particle sizes of the tFNAs and A-T-M were ≈6.492 nm and 14.04 nm, respectively. For the zeta potential, both the tFNAs and A-T-M were negatively charged (−2.68 mV and −6.75 mV, respectively), indicating that A-T-M has a stable

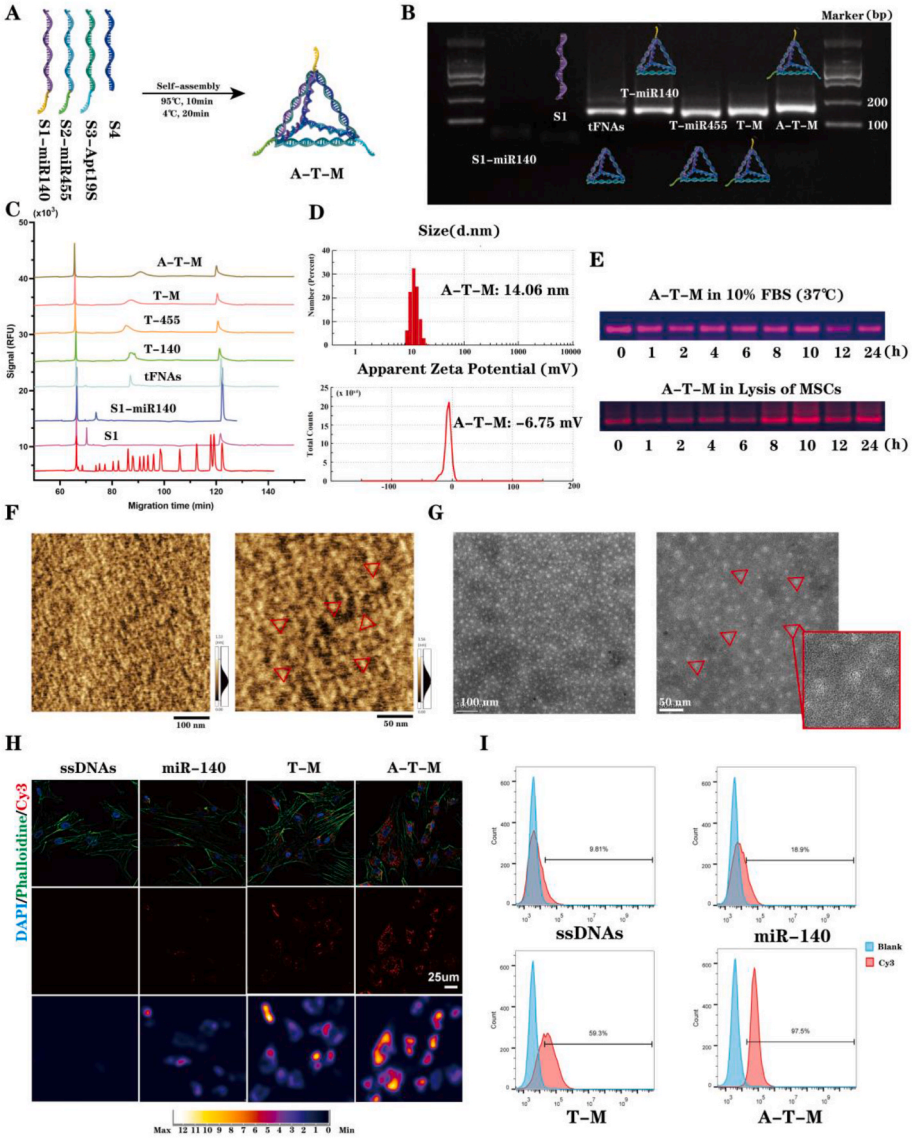

Fig. 2. Preparation, Characterization and Cellular Uptake of A-T-M. A) Diagram of A-T-M synthesis. B) The successful synthesis of tFNAs, T-M and A-T-M was verified by 8 % PAGE. C) HPCE confirmed the successful self-assembly of tFNAs, T-M and A-T-M. D) The particle size and zeta potential of A-T-M detected by a nanoparticle potentiometer and DLS. E) The structural stability of A-T-M in FBS and after MSC lysis. F) Molecular structure of A-T-M imaged using AFM. Scale bar: 100 nm and 50 nm. G) TEM images of the molecular structure of A-T-M. Scale bars: 100 nm and 50 nm. H) The uptake of ssDNA, miRNA, T-M and A-T-M by SMSCs after 12 h was detected via confocal laser scanning microscopy. Scale bar: 25 μm. I) Flow cytometry was used to evaluate the uptake of ssDNAs, miRNAs, T-M and A-T-M by SMSCs.

structure consistent with that of the tFNAs. Moreover, the shape of A-T-M in aqueous buffer was determined by atomic force microscopy (AFM, Fig. 2F) and transmission electron microscopy (TEM, Fig. 2G). The structure of A-T-M was similar to a triangle, and A-T-M was uniformly distributed in aqueous buffer. In addition, the structural stability of A-T-M is crucial for its viability as an optimal nanobiocarrier. Therefore, we assessed the stability of A-T-M in 10 % fetal bovine serum (FBS) and after MSC lysis (Fig. 2E). The results demonstrated that A-T-M exhibited robust stabilization in 10 % FBS and MSC lysis medium for a minimum duration of 24 h, which was deemed optimal for the efficient delivery of miRNAs to MSCs. In summary, the integration of aptamers with tFNAs results in highly functionalized biomolecular systems. As artificial oligonucleotides, aptamers are widely used in the functionalization of nanomaterials and targeted drug delivery due to their impressive affinity for specific targets, ease of synthesis, and rapid tissue penetration [41–43]. Thererore, the application of aptamer Apt19S has significantly improved the off-target effects of tFNA-based miRNA delivery systems. Furthermore, these nanostructures are not only effective but also align with the principles of green biomaterials, emphasizing sustainable synthesis, biodegradability, biocompatibility, and reduced environmental impact [44].

2.2. Cellular internalization and biocompatibility of A-T-M

To verify the ability of A-T-M to transport miRNAs to MSCs, we linked miR-140 to cyanine 3 (Cy3) and synthesized Cy3-T-M and Cy3-A-T-M with Cy3-miR140. Furthermore, SMSCs were incubated with Cy3-ssDNAs, Cy3-miR140, Cy3-T-M or Cy3-A-T-M for 12 h, and confocal laser microscopy and flow cytometry were subsequently performed to determine the cellular uptake rate. Confocal fluorescence images (Fig. 2H and Fig. S4, Supporting Information) showed that pure ssDNAs and pure miR-140 could barely enter the SMSCs, while T-M could be transported into the cells in large quantities without the need for any transfection reagents. Importantly, during the same incubation time, A-T-M loaded with Apt19S had a greater cellular uptake rate than T-M. Similarly, the quantitative results of flow cytometry (Fig. 2I) also showed that 97.5 % of the SMSCs absorbed A-T-M and that 59.3 % of the SMSCs absorbed T-M after incubating for 12 h, while the proportions of cells that absorbed ssDNAs and miR-140 were only 9.81 % and 18.9 %, respectively. These results suggested that tFNAs could successfully transport miRNAs into MSCs, especially after modification by Apt19S, whereas miRNAs alone were difficult to be internalized by MSCs, indicating that A-T-M had the highest affinity for MSCs compared to the other molecules.

We next tested the biocompatibility of A-T-M. According to previous methods [45,46], SMSCs were treated with miRNAs (250 nmol of miR-140 and 250 nmol of miR-455), tFNAs, T-M and A-T-M, and cytotoxicity was analyzed via CCK-8 kits (Fig. S5, Supporting Information). The results showed that the formulations used in these tests had no cytotoxicity, and the tFNAs, T-M and A-T-M also promoted the proliferative activity of the cells. In addition, previous studies have shown that tFNAs can promote the migration of MSCs to a certain extent [37,47]. Therefore, we used wound healing experiments to test whether A-T-M could affect the ability of tFNAs to improveMSC migration (Figs. S6 and S7, Supporting Information). Scratch images at 0, 12 and 24 h indicated that T-M and A-T-M had no effect on the promotion of MSC migration by the tFNAs itself and that A-T-M enhanced the effect of the tFNAs on MSC migration due to the Apt19S modification. Thus, A-T-M can be considered an efficient and safe miRNA codelivery system that can be rapidly internalized by MSCs and increase the effectiveness of tFNAs, which is the premise of using tFNAs as nanocarriers and the key for A-T-M to play an important biological role in MSCs.

2.3. The synergistic effect of miR-140 and miR-455 in regulating SMSC chondrogenic differentiation

In our initial experimental study, we first used quantitative real-time polymerase chain reaction (RT−PCR) to explore the changes in the expression of miR-140 and miR-455 in SMSCs cultured with tFNAs-miR140 (T-140), tFNAs-miR455 (T-455), T-M, or A-T-M. The RT−PCR results showed that the miRNAs in each group were successfully delivered to SMSCs compared to those in the control group, and the increases in the expression of miR-140 and miR-455 in the A-T-M group (47.58-fold and 34.89-fold) were the greatest, indicating that more miRNAs were delivered to SMSCs (Fig. 3B).

We then used Alcian blue (AL) staining (Fig. 3C) to explore the effects of T-140, T-455, T-M, and A-T-M on the increase in the chondrogenic differentiation potential of SMSCs in 2-dimensional (2D) tissue culture plates and measured the corresponding gene expression levels of Sox9, ACAN, and Col2a1 (Fig. 3D). In detail, the statistical analysis of PCR showed that the gene expression levels of Sox9, ACAN, and Col2a1 in the A-T-M group are 10.12, 68.59, and 28.10 times that of the control group, respectively. The experimental data suggested that the codelivery system, which included T-M and A-T-M, was more effective at promoting cartilage differentiation in SMSCs than was the individual delivery of miR-140 and miR-455 by T-140 and T-455, respectively. The above preliminary experimental results confirmed that miR-140 and miR-455 have synergistic effects on the chondrogenic differentiation of MSCs, which has never been reported before (Tables S6 and S7). Therefore, the miRNA codelivery system based on T-M and A-T-M was used for follow-up experimental exploration in this study without focusing on individual delivery, including T-140 and T-455.

2.4. A-T-M orients the differentiation of SMSCs to a hyaline cartilage phenotype

Previous studies have indicated that native joint-resident MSCs play a key role in cartilage regeneration [48]. Specifically, SMSCs may be the primary drivers of AC repair in adults [16]. Following an AC injury, many MSCs are recruited to the site of injury. In the presence of a local regenerative microenvironment, these recruited MSCs undergo differentiation into chondrocytes, which in turn promotes the endogenous repair of cartilage tissue [14,49]. Consequently, it is of utmost importance to precisely control the differentiation fate of MSCs while developing strategies for cartilage regeneration.

The chondrogenic differentiation of MSCs within the joint cavity often relies on specific growth factors found in the local microenvironment following injury, including bone morphogenetic protein (BMP), insulin-like growth factor (IGF), and transforming growth factor-β (TGF-β) [50,51]. Notably, members of the TGF-β superfamily, such as TGF-β1 and TGF-β3, play pivotal roles [52]. However, when intra-articular inflammation occurs and the microenvironment is disrupted, the differentiation of MSCs tends to proceed toward hypertrophic cartilage instead of hyaline cartilage [53]. This process leads to a decrease in the overall function of the regenerated tissue, which is one of the main reasons for the unsatisfactory long-term effectiveness of microfracture surgery [54]. Here, A-T-M was applied to a 3D spheroid culture model of SMSCs induced by TGF-β3 to investigate whether A-T-M can promote the chondrogenic differentiation of MSCs while inhibiting hypertrophic degeneration.

We determined the effects of tFNAs, pure miRNAs, T-M and A-T-M on SMSC chondrogenic differentiation in a 3D spheroid culture model induced by TGF-β3 at different time points (14, 21, and 28 days; Fig. 4A). The expression of chondrogenesis-specific genes (Sox9, Col2a1, and Acan) in each group was determined by RT−PCR at 14 and 21 days (Fig. 4B). Compared with those in the pure TGF-β3-induced group (regular chondrogenic differentiation medium), the spheroids treated with 250 nm A-T-M exhibited the highest expression of Sox9 (2.67-fold and 3.33-fold), Col2a1 (7.05-fold and 16.19-fold), and Acan (9.53-fold

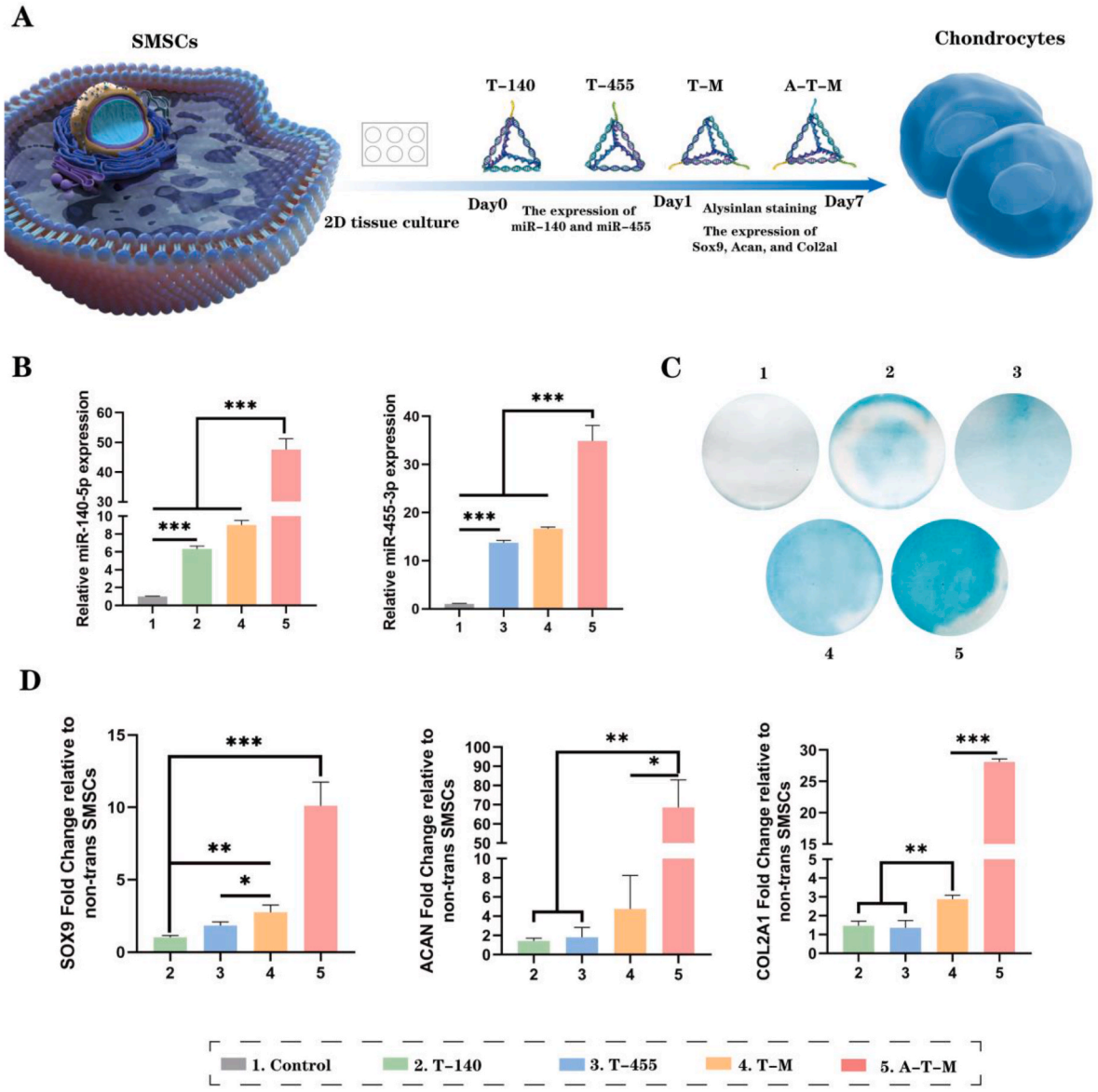

Fig. 3. The Synergistic Role of miR-140 and miR-455 in Regulating SMSC Chondrogenic Differentiation. A) Schematic diagram of SMSC chondrogenic differentiation on 2D tissue culture plates. B) The expression of miR-140-5p and miR-455-3p in each group was determined by RT−PCR. C) Images of SMSC chondrogenic differentiation on 2D tissue culture plates after AL staining on day 7. D) Gene expression of Sox9, Col2a1, and Acan in each group, as shown by RT−PCR. The data are presented as the mean ± SD (n = 3). Statistical analysis: *p < 0.05, **p < 0.01, ***p < 0.001.

and 20.05-fold) at both time points. We subsequently performed histopathological staining, including H&E, safranin O (SO), and AL staining, to assess the morphology of the chondrogenic spheroids 21 days after induction (Fig. 4C and D). The H&E images suggested that spheroids in the A-T-M group were the most deeply stained, indicating that additional extracellular matrix (ECM) was produced. Furthermore, the results of SO and AL staining, which reflect the polysaccharide content, revealed that polysaccharide accumulation in the ECM of SMSCs decreased after A-T-M treatment. The protein expression of Col2 and Acan was determined by immunohistochemistry and immunofluorescence staining, respectively. Compared with those of the control, the spheroids treated with A-T-M exhibited the strongest Col2 and Acan expression at 21 days. Therefore, A-T-M could significantly promote chondrogenic differentiation of SMSCs. Interestingly, we also found that pure tFNAs could enhance the induction of differentiation by TGF-β3 to a certain extent, which was consistent with our previous results [37].

Degenerate chondrogenic differentiation is pivotal for the therapeutic efficacy of MSCs both in vivo and in vitro. Following cellular senescence and inflammation, specific markers such as Col10, Runx2, and MMP-13 accumulate, leading to the gradual emergence of a hypertrophic chondrocyte differentiation phenotype [17]. Compared to hyaline chondrocytes, hypertrophic chondrocytes can further exacerbate joint structure and function deterioration. Hence, RT−PCR (Fig. 4F) and immunofluorescence staining (Fig. 4E) were used to assess the mRNA and protein expression levels of the hypertrophy-specific markers Col10, Runx2, and MMP-13 in the chondrogenic spheroids from each treatment group after 28 days. A-T-M significantly downregulated the expression of Col10, Runx2, and MMP-13 in chondrogenic spheroids, indicating that A-T-M successfully inhibited the degenerative process during chondrogenesis. Furthermore, we investigated the effects of A-T-M on SMSC chondrogenic differentiation in a 3D spheroid culture model under intra-articular inflammation mimic microenvironment. Pathological staining and PCR results (Fig. S8) showed that under IL-1β stimulation, the chondrogenic ability of SMSCs was significantly inhibited, accompanied by evident hypertrophic differentiation. However, A-T-M allso significantly reversed this process, indicating its

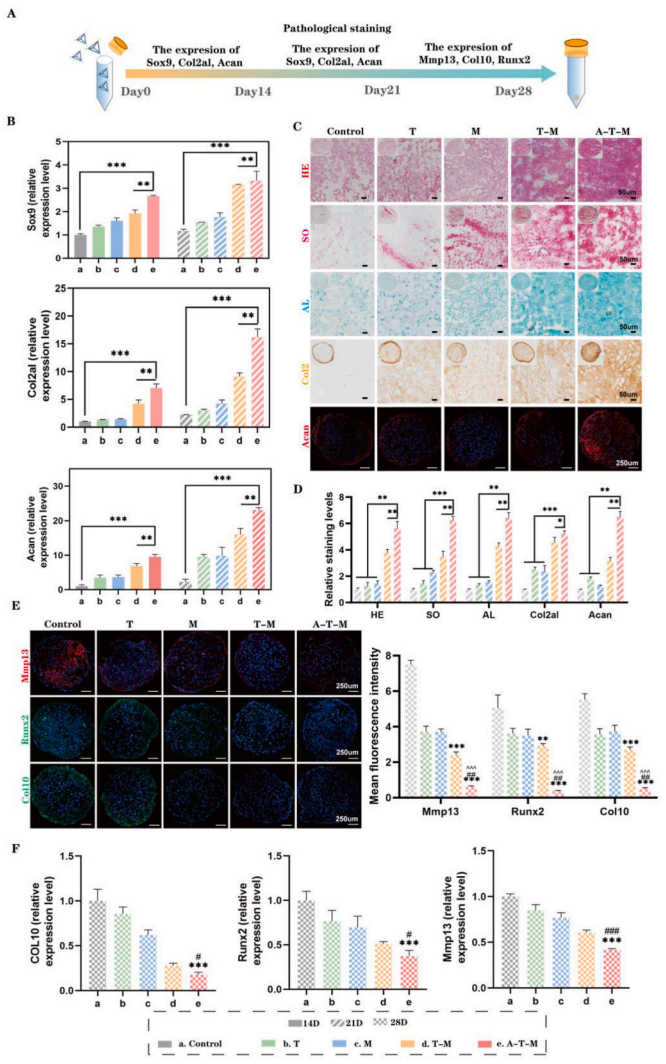

Fig. 4. A-T-M Promotes the Chondrogenic Differentiation of SMSCs to a Hyaline Cartilage Phenotype A) Schematic diagram of the 3D spheroid culture model of SMSCs treated with A-T-M. B) Gene expression of Sox9, Col2a1, and Acan in each group at 14 and 21 days as shown by RT−PCR. C) H&E, SO, AL, and immunohistochemical staining of Col2 and immunofluorescence staining of Acan in single spheroids from different groups on day 21. D) Quantitative analysis of H&E, SO, AL, and immunohistochemical staining of Col2 and immunofluorescence staining of Acan. Scale bars: 50 μm and 250 μm. E) Immunofluorescence staining images and quantitative analysis (of MMP-13, Runx2, and Col10) of single spheroids from different groups on day 28. Scale bar: 250 μm. F) Gene expression of Col10, Runx2, and MMP-13 in each group at 28 days, as shown by RT−PCR. The data are presented as the mean ± SD (n = 3). Statistical analysis: *p < 0.05, **p < 0.01, ***p < 0.001 (Groups: *: control, #: tFNAs).

effective role even in an inflammatory environment.

Based on these results, A-T-M may promote the differentiation of MSCs into chondrocytes after cartilage injury. At the late differentiation stage, MSCs derived from defects may secrete Col10, Runx2, and MMP-13, which are involved in cartilage degeneration. However, A-T-M intervention can inhibit this degeneration via chondrogenesis and trigger the generation of hyaline cartilage, which helps to reconstruct the microenvironment during AC regeneration.

2.5. A-T-M enhances HIF1α and FOXO signaling, promoting the chondrogenic differentiation of SMSCs

To further explore the mechanism by which A-T-M acts on SMSCs, we performed mRNA sequencing analysis of two groups of SMSCs treated with or without A-T-M for 24 h. As shown in Fig. 5A and B, principal component analysis (PCA) and a Venn diagram of gene expression levels demonstrated a discernible distinction between the two sample groups and confirmed the reproducibility of the samples within each group. Compared to those in the control group, 180 differentially expressed genes (DEGs) were identified in the A-T-M group [false discovery rate (FDR) < 0.05, |log2 (fold change A)|>1], with 77 upregulated genes and 103 downregulated genes (Fig. 5C and D). Gene Ontology (GO) analysis of the two groups revealed that the DEGs were strongly correlated with cholesterol biosynthesis, cytokine secretion, response to hypoxia, and ECM accumulation (Fig. 5E).

Moreover, Kyoto Encyclopedia of Genes and Genomes (KEGG) pathway analysis of the A-T-M and control groups suggested that functional pathways associated with lipid metabolism, hypoxia, MAPK, Ras, PI3K/Akt and other functional pathways relevant to chondrogenic differentiation were enriched (Fig. 5F and G). Gene set enrichment analysis (GSEA) further verified that with the addition of A-T-M, the lipid metabolism-related functions of SMSCs, including fatty acid biosynthesis and the forkhead box O (FOXO) signaling pathway, decreased, and hypoxia-related signaling pathways [hypoxia inducible factor-1α (HIF-1α)] and the classic TGF-β pathway related to chondrogenic differentiation increased (Fig. 5H). Subsequently, we focused on functions related to hypoxia regulation, lipid metabolism and chondrogenic differentiation and found that the expression of HIF-1α, FOXO1, FOXO3 and chondrogenic differentiation-related genes (Tgfb1, Tgfb2, and Tgfb3) was upregulated in the A-T-M group compared to the control group (Fig. 5I and J).

The hypoxia response and lipid metabolism are two important pathways that regulate the differentiation fate of MSCs [55–57]. HIF-1α, a key mediator of the cellular response to hypoxia, has been shown to promote the chondrogenic differentiation of MSCs by upregulating the expression of SOX9, the critical transcription factor involved in chondrogenesis [58]. In addition, Nick van Gastel et al. revealed that FOXO transcription factors can bind to the SOX9 promoter and increase its expression, further initiating cartilage formation and inhibiting fatty acid oxidation to regulate cellular lipid metabolism [56]. Therefore, we utilized Western blot (WB) and immunofluorescence staining to evaluate the protein expression levels of HIF-1α, FOXO1, FOXO3, and SOX9 in SMSCs after A-T-M treatment to further validate the results obtained from transcriptome sequencing. The WB results (Fig. 6A and B) indicated that A-T-M significantly upregulated the expression of HIF-1α (1.67-fold), FOXO1 (1.41-fold), FOXO3 (1.48-fold), and SOX9 (1.57-fold) in SMSCs compared to the control group. Similarly, immunofluorescence images (Fig. 6C–F) showed that the fluorescence intensity of the four proteins in SMSCs was greater after A-T-M treatment than after the other treatments. Furthermore, the HIF-1 pathway inhibitor KC7F2 and the FOXO inhibitor AS1842856 prevented induction of SOX9 during A-T-M treatment in SMSCs chondrogenic differentiation (Fig. S10).

In summary, all the findings demonstrated that A-T-M can enhance the chondrogenic differentiation of SMSCs by regulating the HIF-1α signaling pathway and the FOXO signaling pathway to promote the expression of SOX9 (Fig. 6G). As a multifunctional targeted delivery system, A-T-M promoted the migratory ability of SMSCs and regulated their differentiation into hyaline chondrocytes, paving the way for enhancing the endogenous regeneration of AC.

2.6. A-T-M enhanced the endogenous repair capacity of AC in rats

We intra-articularly injected Cy3-labeled miR-140, T-M, and A-T-M into the knees of the rats to evaluate the distribution and retention of T-M and A-T-M in vivo. The images acquired by an in vivo fluorescence imaging system at seven different time points (0, 15, 30, 45, 60, 90, and 120 min) after intra-articular injection (Fig. S11, Supporting Information) demonstrated that the fluorescence intensity of the Cy3-T-M and

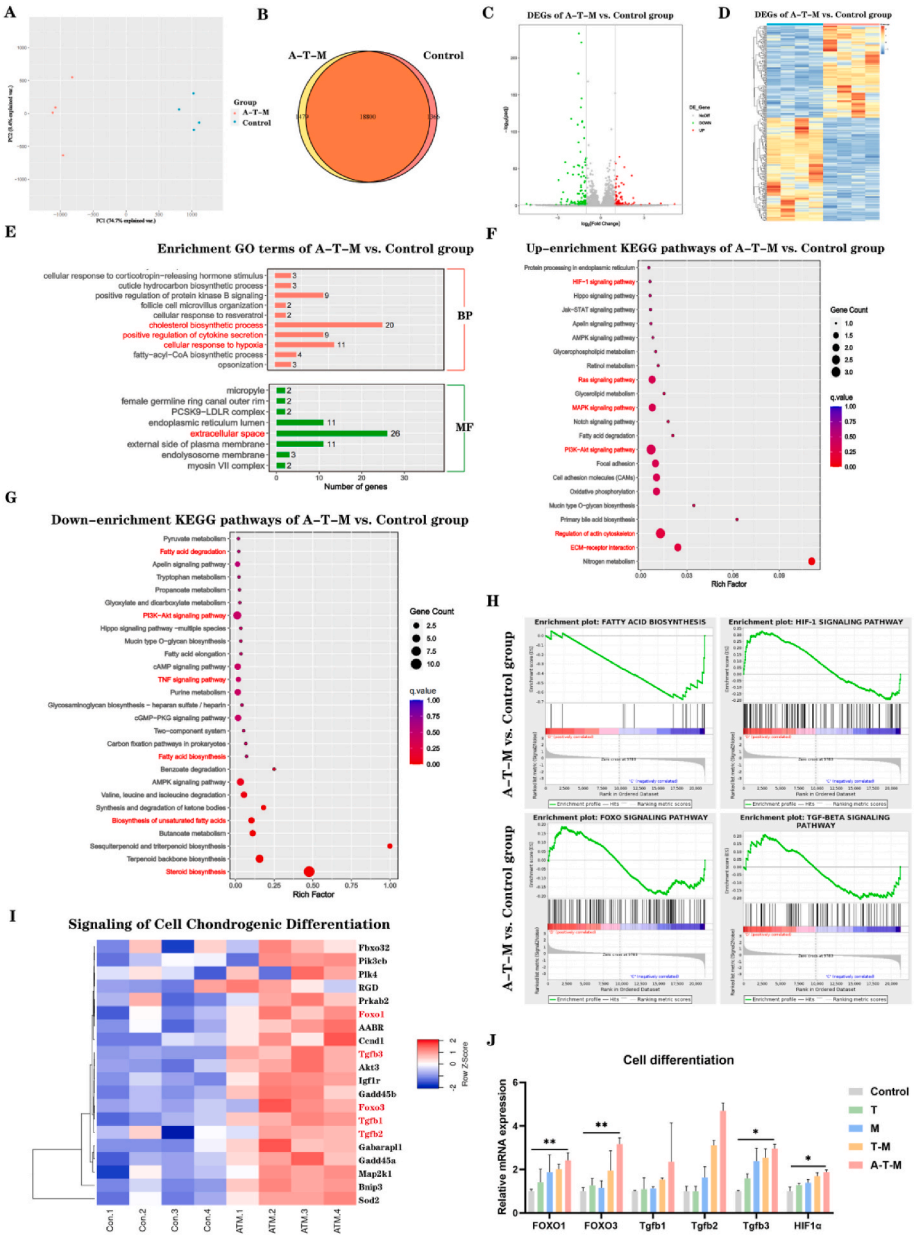

Fig. 5. Intrinsic Mechanisms of A-T-M on SMSC Behavior. A) PCA of the samples in the two groups (n = 4). B) Venn diagram of gene expression between the two groups. C) Scatter plot and D) cluster analysis of DEGs between the two groups. E) GO enrichment bar plots of DEGs. F) KEGG enrichment bar plots. G) KEGG inhibition bar plots. H) GSEA enrichment analysis of fatty acid biosynthesis, the HIF-1 signaling pathway, the FOXO signaling pathway, and the TGF-BETA signaling pathway between the A-T-M and control groups. I) Heatmap of genes related to cell chondrogenic differentiation. J) qRT–PCR analysis of genes associated with cellular hypoxia regulation and chondrogenic differentiation. The data are presented as the mean ± SD (n = 3). Statistical analysis: *p < 0.05, **p < 0.01.

Cy3-A-T-M groups was greater than that of the free Cy3-miR-140 group over time. In addition, Cy3-A-T-M showed the greatest retention in the joint at 120 min after intra-articular injection, indicating that the Apt19S-modified tFNAs greatly enhanced the stability and effective time of the miRNAs in the joint.

We then established a chondral defect model in rats (diameter: 2 mm, depth: 1 mm) based on previous methods for in vivo research to gain a deeper understanding of the effects of various treatments on AC endogenous repair [59,60]. After the model was established, the same volume of normal saline (negative control), tFNAs, miRNAs (250 nmol of miR-140 or 250 nmol of miR-455), T-M and A-T-M was immediately injected into the knee cavity once every 3 days for 12 weeks. Fig. 7A shows a schematic diagram of the chondral defect model in rats and treatment with A-T-M for 12 weeks. After intra-articular injection of Cy3-labeled miRNAs, T-M, and A-T-M, immunofluorescence was performed to evaluate the affinity of the A-T-M for MSCs within the first week post-surgery. Regenerated tissue from the defect was collected, and MSCs were specifically immunofluorescently labeled with the CD90 marker. Fluorescence was detected by confocal microscopy (Fig. 7B), and the results of the quantitative analysis of CD90 and Cy3 double-positive cells (Fig. 7C) showed that, compared with that in the control and T-M groups, a greater amount of red Cy3 fluorescence was observed in the ATM group, which significantly overlapped with the green fluorescence signal of MSCs. These findings indicate that the injection of A-T-M significantly increases the number of MSCs at the defect site and that the introduction of aptamers in tFNAs can substantially enhance the affinity for MSCs. In addition, tFNAs improved the in vivo migration of MSCs to the defect site and the delivery efficiency of miRNAs to cells, which was consistent with the results of previous studies [37,47]. In cases of AC injury, mobilizing endogenous MSCs to

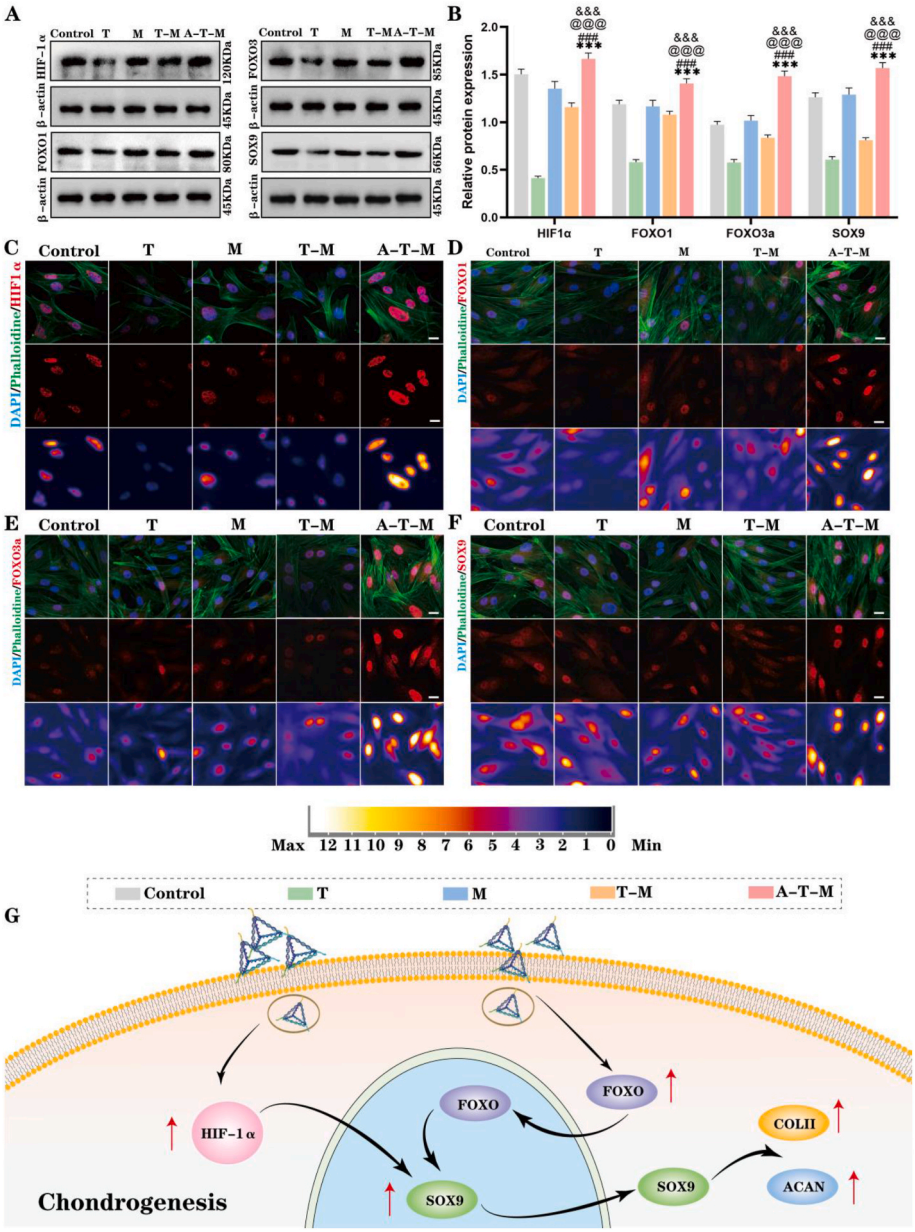

Fig. 6. A-T-M Promotes the Chondrogenic Differentiation of SMSCs by Enhancing HIF1α and FOXO Signaling A) WB was used to determine the protein expression of SMSCs (HIF-1α, FOXO1, FOXO3, and SOX9) under different treatment conditions. B) Quantitative analysis of the WB results. C–F) Immunofluorescence detection of HIF-1α, FOXO1, FOXO3, and SOX9. Scale bar: 25 μm. G) Schematic diagram of the changes in SMSC chondrogenic differentiation promoted by A-T-M. The data are presented as the mean ± SD (n = 3). Statistical analysis: ***p < 0.001 (Groups: *: control, #: T, @: M, &: T-M).

the defect site is crucial for early repair. Notably, the endogenous regeneration of articular cartilage relies on various types of mesenchymal stem cells rather than the action of a single cell type. The in vivo target of A-T-M is not limited to SMSCs but broadly affects BMSCs. These results demonstrated that A-T-M achieved targeted miRNA delivery to MSCs in vivo and mobilized enough endogenous MSCs to the defect site, providing a solid foundation for subsequent cartilage regeneration.

Rats were sacrificed at 6 and 12 weeks post-surgery for macroscopic evaluation, microcomputed tomography (micro-CT), pathological staining, and immunohistochemical analysis (Fig. 7A). As shown in Fig. 7D, the appearance of the retrieved rat femoral trochlear samples indicated that the control group, tFNA (T) group, and miRNA (M) group still exhibited significant depressions in the regeneration area, with uneven surfaces of the newly formed tissue and notable color differences compared to the surrounding normal cartilage tissue at 6 and 12 weeks post-surgery. Compared with those in the first three groups, the regenerated tissue in the T-M group was closer to normal cartilage, but there was still a distinct boundary with the surrounding tissue. The regenerated tissue of the A-T-M group was significantly superior to that of the other four groups, showing better integration and consistency with the surrounding normal tissue. Based on the criteria provided by the International Cartilage Repair Society (ICRS) for macroscopic evaluation (Table S3, Supporting Information), the samples from each group were scored at 6 and 12 weeks post-surgery. The ICRS score (Fig. 7E) and heatmap analysis (Fig. 7F) suggested that the regenerated cartilage tissue of the A-T-M group had the highest ICRS overall scores at both 6 and 12 weeks post-surgery. Furthermore, micro-CT analysis and 3D reconstruction were performed to assess the regeneration of subchondral bone at the defect site. As shown in Fig. 7G, at 6 weeks post-surgery, the control group, T group and M group contained only a small amount of newly formed bone, demonstrating limited repair capability. The T-M group and A-T-M group exhibited more consistent subchondral bone

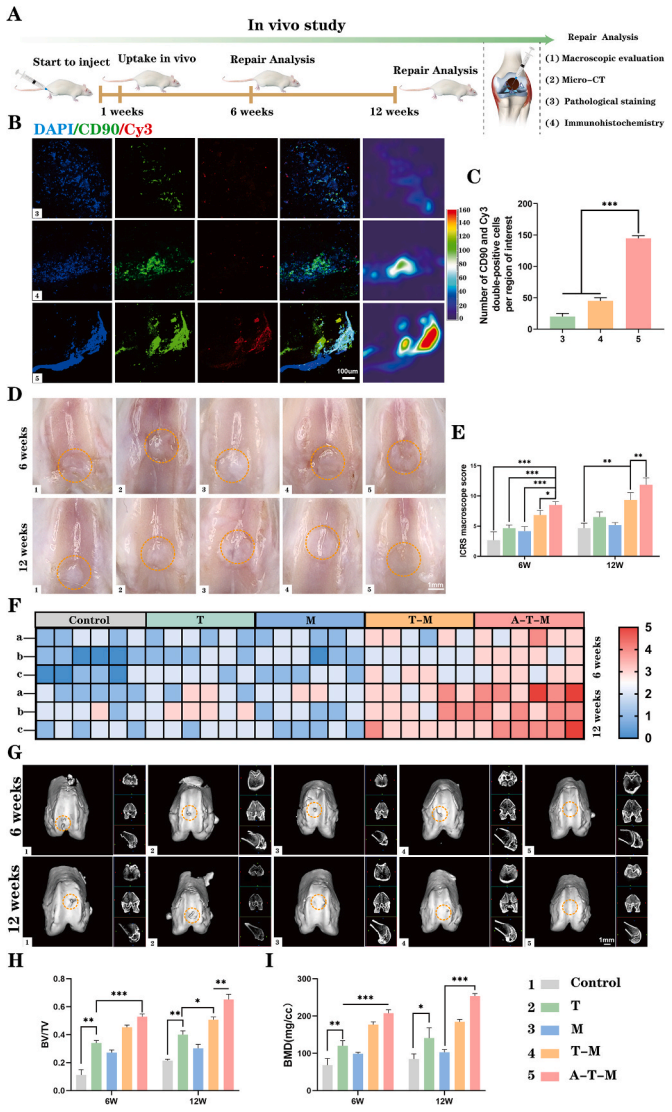

Fig. 7. A-T-M Promotes the Endogenous Repair of AC in SD Rats. A) Schematic diagram of the chondral defect model and treatment with A-T-M in rats. B) Immunofluorescence images of Cy3+/CD90+ cells at the defect sites taken by confocal microscopy at 1 week post-surgery. C) Quantitative analysis of Cy3+/CD90+ cells at the defect sites. D) The gross appearance of the different groups at 6 and 12 weeks post-operation. E) The ICRS macroscopic repair score. F) Heatmap of the ICRS score (a: degree of defect repair, b: integration into the border zone, c: macroscopic appearance). G) The reconstructed micro-CT images. H) Quantitative analysis of the BV/TV in the ROIs. I) Quantitative analysis of the BMD in the ROI. The data are presented as the mean ± SD (n = 3). Statistical analysis: *p < 0.05, **p < 0.01, ***p < 0.001.

repair. At 12 weeks post-surgery, the formation of subchondral bone in the control group, T group, M group and T-M group improved compared to that at 6 weeks post-surgery but still showed significant defects. At 12 weeks, the A-T-M group displayed the most continuous and complete subchondral bone regeneration. Subsequently, we selected the region of interest (ROI) to measure the bone volume/tissue volume (BV/TV; Fig. 7H) and bone mineral density (BMD; Fig. 7I) of the target regenerated tissue. The results indicated that the control group had the lowest BV/TV and BMD values at both 6 and 12 weeks, while the ATM group achieved the best results at both time points.

To further confirm the therapeutic effect of A-T-M, we performed various histological examinations (H&E, SO/Fast Green, toluidine blue, and Col2 immunohistochemical staining) to assess the repaired tissue histopathology at 6 and 12 weeks post-surgery. H&E staining (Fig. 8A) revealed that, in the control group, no new tissue filled the defect, and this finding was accompanied by collapse of the subchondral bone and fibrous tissue filling the collapsed cavity. In the T and M groups, partial new tissue filling was observed with uneven surfaces, distinct boundaries, and disorganized arrangement of spindle-shaped fibroblasts and a few rounded chondrocytes in the filling tissue. The T-M group showed completely filled cartilage-like tissue, which was thinner than the surrounding cartilage and had a slightly rough surface. The A-T-M group showed completely filled cartilage-like tissue, which was thinner than the surrounding cartilage and had a smooth surface. The distribution of the proteoglycans was investigated by SO/Fast Green (Fig. 8B) and toluidine blue (Fig. 9A) staining. Compared with the other four groups, the A-T-M group had the greatest amount of positive staining at both time points, indicating that the proteoglycan deposits were most abundant in the ECM. Moreover, immunohistochemical staining was performed to assess Col2 deposition and distribution (Fig. 9B). Compared with those in the control, T, M and T-M groups, the deposition of Col2 in the regenerated tissue was greater in the A-T-M group. Accordingly, Mankin and Wakitani histological scoring (Table S4 and Table S5, Supporting Information) was performed to assess the quality of the regenerated cartilage in each group based on histopathological staining at 12 weeks post-surgery. A heatmap analysis (Fig. 9C) and total score (Fig. 9E and F) of the histological score showed that the regenerated cartilage was better in the A-T-M group than in all the other groups (a better regenerative effect indicated a lower score). Notably, significant differences were observed between the A-T-M dataset and other datasets via PCA, suggesting that there were significant histological differences between the A-T-M group and the other groups undergoing cartilage repair (Fig. 9D). Specifically, the histological scores of individual parameters further demonstrated that the application of A-T-M significantly enhanced the individual parameters “structure”, “cellularity”, “cell morphology”, “surface regularity”, “matrix staining”, and “thickness of cartilage” (Fig. 9G–L).

In the following work, the distribution and orientation of regenerated collagen fibers in the newly formed cartilage tissue after 6 and 12 weeks of repair were observed using Sirius Red staining and polarized light microscopy (Fig. 10A and Fig. S12). Collagen fiber tissue is a crucial factor determining the biological function and mechanical performance of AC [61]. Previous studies have shown that the collagen fibers in the surface area of normal AC are arranged in an orientational parallel-aligned arrangement, while those in the deep basal area are arranged vertically [62]. Therefore, the orientation of regenerated collagen fibers in two different regions (including surface and deep zones) at 12 weeks was analyzed using ImageJ software, as depicted in Fig. 10B and C. The control and M groups exhibited irregular distributions of collagen fibers on both the surface and in deep zones, whereas the T and T-M groups showed some orientation. In the ATM group, the most parallel-aligned arrangement was observed in the surface zone, and the most vertical-aligned arrangement was observed in the deep zone close to the normal cartilage.

To verify whether A-T-M can still inhibit the degeneration of MSC chondrogenic differentiation in vivo, we employed immunohistochemistry and immunofluorescence to examine the expression of MMP13, Col10, and Runx2, which are characteristic markers of chondrocyte aging and hypertrophy (Fig. 10D and E). There was almost no expression of MMP13, Col10, or Runx2 in the regeneration area of the A-T-M group compared with that in the other groups, demonstrating that the application of A-T-M successfully inhibited the generation of hypertrophic chondrocytes. In addition, we performed H&E staining of the major organs (heart, liver, spleen, lung, and kidney) of the rats in the different groups at 12 weeks post-surgery to assess the biosafety of A-T-M in vivo (Fig. S13, Supporting Information). The intra-articular injection of A-T-M did not cause any pathological changes in these organs, indicating that A-T-M not only has good biocompatibility and low biological toxicity but also has excellent potential for clinical translational applications.

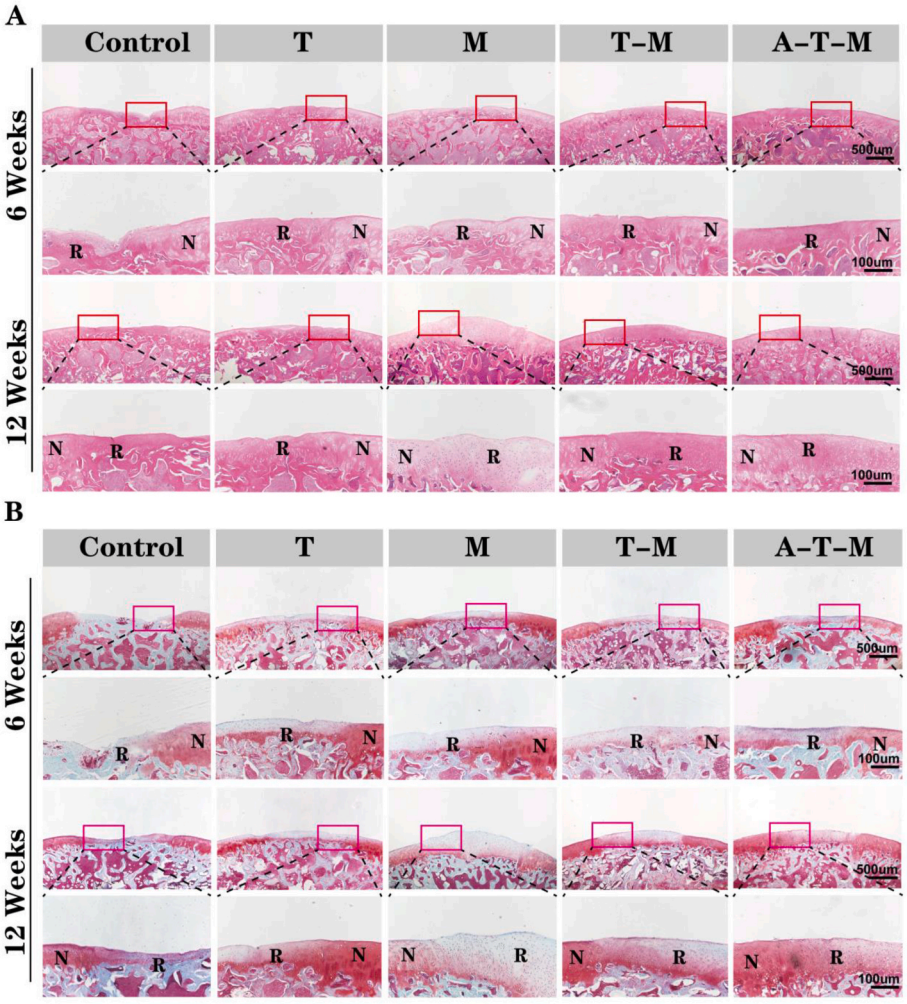

Fig. 8. Histomorphological Evaluation of Repaired Cartilage in SD Rats. A) H&E staining, B) SO/Fast Green staining of the repaired tissue from different groups at 6 and 12 weeks post-surgery (N represents normal cartilage, R represents repaired cartilage). Scale bars: 100 μm and 500 μm.

Based on these results, A-T-M significantly enhances the endogenous repair ability of rat knee joint cartilage after injury and successfully blocks the hypertrophy of MSCs during the chondrogenic formation process, which further improves the quality of regenerated cartilage. The long-term stability and effectiveness of the regenerated cartilage tissue in vivo, especially under normal wear and physiological stresses, are crucial for cartilage repair. In the process of cartilage repair, the formation of fibrocartilage significantly affects the surface lubrication and mechanical strength of the cartilage, leading to accelerated wear of regenerated cartilage tissue and increased risk of re-injury. Our preliminary experimental results have indicated that the A-T-M system can inhibit the formation of fibrocartilage. We will further assess the long-term lubrication and mechanical properties, including tensile strength, compressive modulus, and elasticity, of regenerated cartilage tissue following extended A-T-M treatment cycles, and then compare them with natural cartilage. In addition, we selected rats at 6–8 weeks of age for in vivo experiments. Selecting this age range helps ensure consistency and reliability in the results, as the animals are at a relatively uniform stage of development, reducing variability related to age-dependent changes in physiology. On the other hand, this allows the assessment of the treatment efficacy in a biological context that mirrors active regenerative processes, which is crucial for understanding the potential benefits and mechanisms of the treatment in a scenario where natural repair mechanisms are still operational. However, the high potential for self-healing in this age group may influence the outcomes. In future work, we plan to include older rats to mitigate the self-healing effect and to provide a comparison across different age groups.

The development of more safe and efficient treatment strategies has became a crucial research topic in the field of articular cartilage tissue engineering. Compared to existing treatments like microfracture techniques, autologous chondrocyte implantation (ACI) or other biomaterial-based approaches, the A-T-M system is designed to be cost-effective and application-easy by utilizing a single-stage procedure and off-the-shelf materials that do not require extensive cell manipulation or culturing. Certainly, following preclinical large animal validation, we will design rigorously controlled clinical trials to compare patient outcomes between the A-T-M system and traditional treatment methods. In addition, we aslo will design rigorous control experiments to compare the dual-miRNA system to other miRNA delivery systems including viral vectors, liposomes, and other nanoparticle-based carriers, underscoring the enhanced effectiveness of the dual-miRNA approach in promoting cartilage regeneration. We believe this future comprehensive evaluation couldsupports the potential of our system as a superior alternative in cartilage repair research. Furthermore, an important limitation affecting the application of the A-T-M system is large-scale production. The synthesis process of the tFNA-miRNA complex has been optimized for reproducibility and efficiency on a laboratory scale, using readily available reagents and standard equipment, suggesting good potential for upscaling. However, ensuring the consistency of oligonucleotide and miRNA reagent quality during large-scale production and maintaining

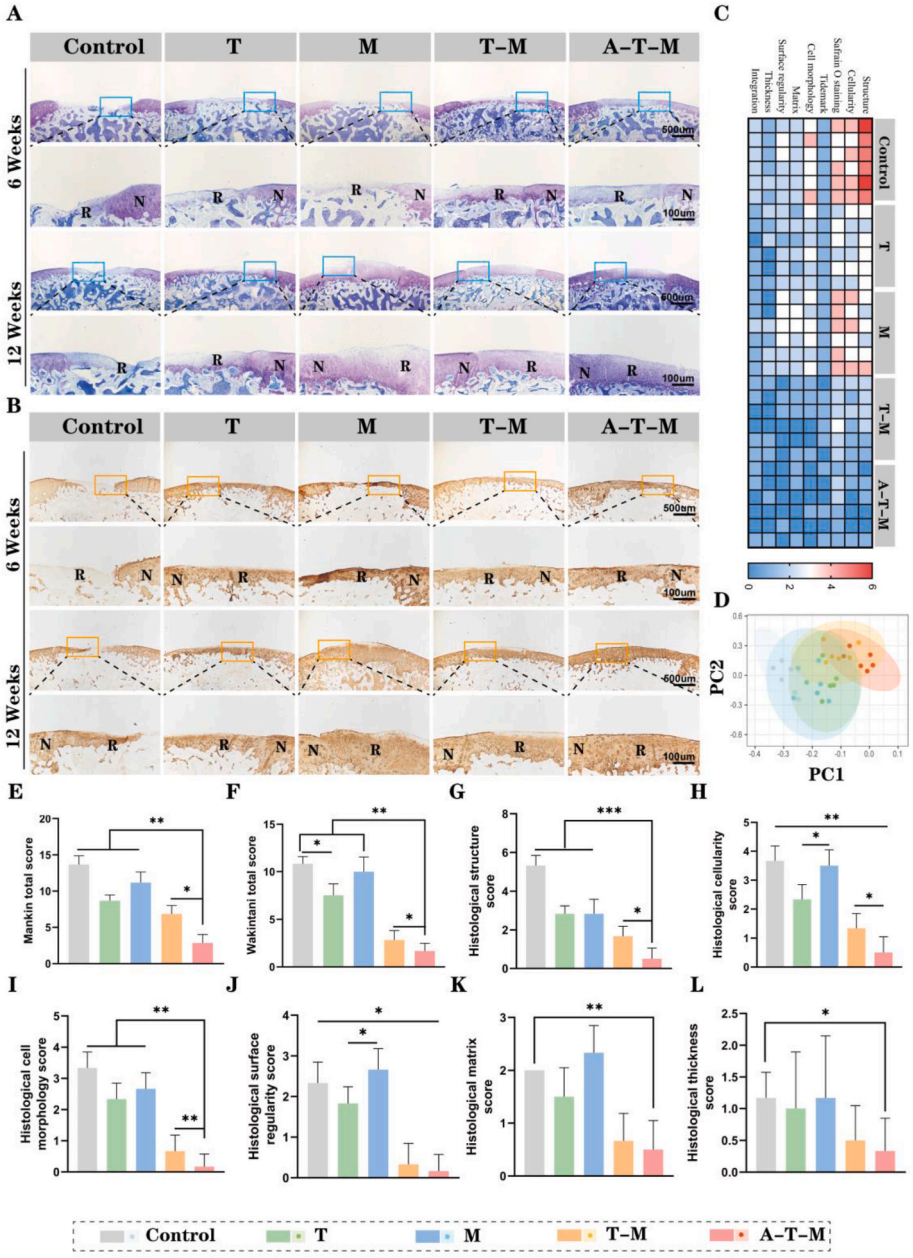

Fig. 9. Histomorphological Evaluation of Repaired Cartilage in SD Rats. A) toluidine blue staining, and B) type-II collagen immunohistochemical staining of the repaired tissue from different groups at 6 and 12 weeks post-surgery (N represents normal cartilage, R represents repaired cartilage). Scale bars: 100 μm and 500 μm. C) Heatmap of the histological parameters. D) PCA of histological scores among groups. E) Mankin histological total score. F) Wakitani histological total score. G) Histological structure score. H) Histological cellularity score. I) Histological cell morphology score. J) Histological surface regularity score. K) Histological matrix staining score. L) Histological thickness of the cartilage score. The data are presented as the mean ± SD (n = 3). Statistical analysis: *p < 0.05, **p < 0.01, ***p < 0.001.

the integrity of the tFNA-miRNA complex during the purification process pose significant challenges. Despite these challenges, the increasing advancements in nucleic acid synthesis technologies and scalable manufacturing practices provide a promising outlook for the large-scale production of tFNA-miRNA complexes.

3. Conclusion

We constructed a novel aptamer-tFNA delivery system for dual miRNAs to improve current therapeutic strategies for AC injury, denoted A-T-M; this system could incorporate the cellular targeting of Apt19S, the biological advantages of tFNAs, and the cartilage regenerative potential of miR-140-5p and miR-455-3p to enhance chondrogenic differentiation of joint-resident MSCs and inhibit the hypertrophic degenerative process for quality AC endogenous repair. A-T-M significantly protected the stability of miRNAs and had sufficient effects on MSCs, which improved the transmissibility of the tFNAs. A-T-M could enhance the migratory ability of MSCs and increase their number at defective sites, paving the way for endogenous cartilage regeneration. A-T-M could also enhance the HIF-1α and FOXO signaling pathways to promote MSC differentiation into stable chondrocyte phenotypes accompanied by the inhibition of hypertrophic degeneration processes, which promotes precise recovery of cartilage function. In addition, this study demonstrated, for the first time, that miR-140-5p and miR-455-3p had synergistic effects on MSC chondrogenic differentiation. Accordingly, A-T-M represents a new cartilage regeneration strategy with

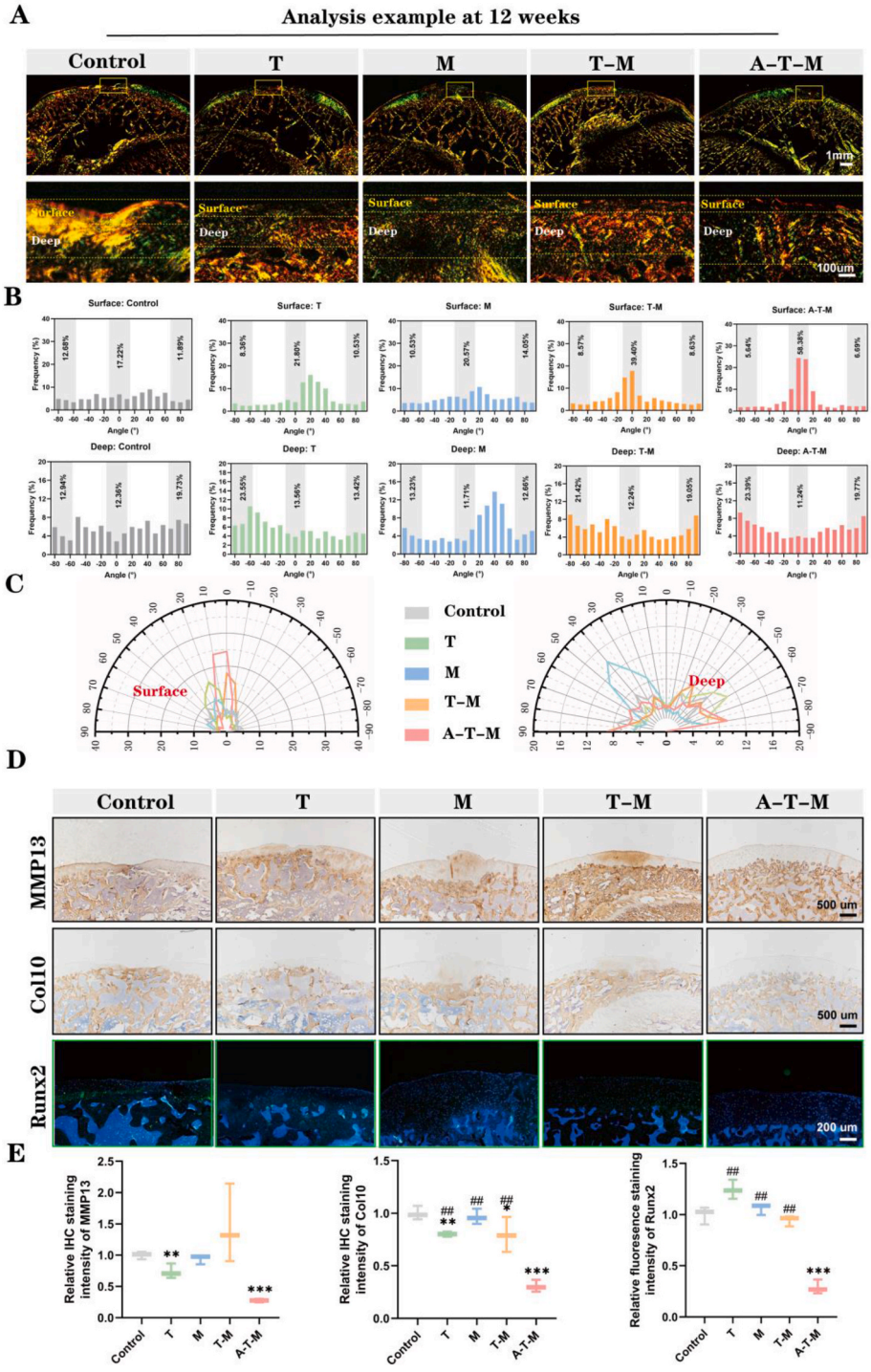

Fig. 10. Evaluation of Collagen Fiber Orientation and Hypertrophic Degeneration of Repaired Cartilage in SD Rats Post-Surgery. A) Polarized light microscopy images of the regenerated area stained with Sirius Red in each group at 12 weeks post-surgery. Scale bars: 1 mm and 100 μm. B) Orientation and dispersion of collagen fibers in the superficial and deep zones at defect sites. C) Polar coordinate analysis of the collagen fiber arrangement in the surface and deep zones. D) Immunohistochemical (for MMP13 and Col10) and immunofluorescence (for Runx2) staining of the repaired tissue from different groups at 12 weeks post-surgery. Scale bar: 500 μm. E) Quantitative analysis of immunohistochemical and immunofluorescence staining. The data are presented as the mean ± SD (n = 3). Statistical analysis: *p < 0.05, **p < 0.01, ***p < 0.001 (Groups: *: control, #: A-T-M).

essential clinical translational value, providing new insight and experimental evidence in regenerative medicine.

4. Experimental section

4.1. Preparation and characterization of tFNAs and A-T-M

As previously described [63,64], tFNAs were rapidly self-assembled from four predesigned ssDNA strands with equimolar concentrations (S1, S2, S3 and S4; Table S1, Supporting Information) through a simple

program (95 °C for 10 min, 4 °C for 20 min). Then, miR-140-5p and miR-455-3p were added to the 3′ ends of S1 and S2, respectively, to form new S1 and S2 (S1-miR140 and S2-miR455, Table S1, Supporting Information), and Apt19S was subsequently added to the 3′ end of S3 (S3-Apt19S, Table S1, Supporting Information). Next, T-140, T-455, T-M and A-T-M were synthesized following the same steps as those used for the tFNAs. The initial concentration of single-stranded DNA containing miR-140 and miR-455 was 100 μM. After synthesizing delivery system in a 1:1 ratio, the concentration was 1 μM, with a final working concentration of 250 nM. Finally, 8 % PAGE, HPCE, DLS, AFM and TEM were performed to verify the successful synthesis and for observation of the structures of A-T-M.

4.2. Cell culture

Rat SMSCs were purchased from Procell (Wuhan, China) and cultured in fresh Dulbecco's modified Eagle's medium (DMEM)/F12 (Corning, USA) supplemented with 10 % FBS (Gibco, USA). The cells were incubated and passaged in a constant temperature incubator (5 % CO_2 and 37 °C). Passages 1 to 3 of SMSCs were used in this study.

4.3. Cell uptake of A-T-M

Cy3-S1, Cy3-miR140, Cy3-T-M and Cy3-A-T-M (250 nm) were cocultured with SMSCs for 12 h. Confocal laser microscopy and flow cytometry were subsequently performed to determine the cellular uptake rate.

4.4. Construction of a 3D spheroid culture model

Three-dimensional cell spheroids were constructed with an SMSC suspension according to our previous study [37]. SMSCs in the experimental group were treated with chondrogenic differentiation induction medium (MSCgoTM; Biological Industries, Israel) containing T, M, T-M, or A-T-M, while those in the control group were treated with pure induction medium. The medium was refreshed every 3 days. The expression of Sox9, Col2a1, and ACAN in the different groups at 7 and 14 days was analyzed via RT−qPCR. After induction for 14 days, H&E staining, SO staining, AL staining and type II collagen immunohistochemical staining were performed to evaluate the degree of chondrogenic differentiation. Finally, RT−qPCR and immunofluorescence staining (for MMP13, Runx2 and Col10) were used to evaluate hypertrophic degeneration at 28 days. A detailed description is provided in the Supporting Information.

4.5. mRNA transcriptome sequencing

See the Supporting Information for a detailed description.

4.6. RT−qPCR

Total RNA was extracted using a total RNA extraction kit (Vazyme, Nanjing, China). The RNA was then reverse transcribed into cDNA using a reverse transcription kit (Vazyme, Nanjing, China). Real-time quantitative RT−qPCR was performed using SYBR Green I PCR Master Mix. The corresponding primer sequences are listed in Table S2 (Supporting Information), with the housekeeping gene GAPDH serving as a control.

4.7. Immunofluorescence assays

The samples were routinely fixed, blocked, and incubated overnight with dilutions of the following primary antibodies: aggrecan (1:200; Invitrogen), MMP13 (1:200; Proteintech), Runx2 (1:100; CST), Col 10 (1:200; Abcam), SOX9 (1:200; Abcam), HIF-1α (1:200; CTS), FOXO1 (1:200; CST), FOXO3 (1:200; Proteintech) and CD90 (1:100; Proteintech). After 40 min of staining with fluorescent secondary antibodies, the nuclei were stained with DAPI, and the cytoskeleton was stained with phalloidin and visualized via fluorescence microscopy.

4.8. Western blotting

After routine protein lysis, denaturation, electrophoresis, and membrane transfer, the membranes were blocked with blocking buffer for 15 min. The membranes were subsequently incubated overnight at 4 °C with the following diluted primary antibodies: anti-β-actin (1:500, Abcam), anti-SOX9 (1:500, Abcam), anti–HIF–1α (1:500, CTS), anti-FOXO1 (1:500, CST), and anti-FOXO3 (1:500, Proteintech). The membrane was incubated with the secondary antibody at room temperature, after which the protein bands were visualized.

4.9. Rat AC defect model

This research was approved by the Institutional Animal Care and Use Committee of PLA General Hospital. Thirty male rats (6–8 weeks old, 250–300g) were randomly divided into five groups (control, T, M, T-M and A-T-M). The rats were anesthetized, and their skin was routinely prepared and sterilized. The left knee joint cavity of the rat was opened, and the femoral trochlea was exposed. A trephine was drilled proximal to the medial collateral ligament in the center of the trochlear groove (diameter: 2 mm, height: 1 mm), and the incision was closed layer by layer. Intra-articular injections were given once every 3 days after surgery. The specimens were harvested at 1, 6, and 12 weeks after surgery.

4.10. Macroscopic evaluation and Micro-CT analysis

The samples (3 animals per group) at 6 and 12 weeks post-surgery were scored according to the ICRS guidelines for macroscopic evaluation (Table S3, Supporting Information). The Explorer Locus SP system (GE, Boston, MA, USA) was subsequently used to scan the samples. Finally, 3D CT reconstruction of femur samples was performed, and the BMD and BV/TV were calculated.

4.11. Histological staining and scores

A detailed description is provided in the Supporting Information.

4.12. Statistical analysis

The mean ± standard deviation (SD) ($n \geq 3$) was used to express the data. One-way analysis of variance (ANOVA) was used to assess the differences between groups, followed by Tukey's multiple testing correction. The statistical software used for the data analysis was GraphPad Prism 8.0 and ImageJ. A p value of less than 0.05 indicated statistical significance.

Ethics approval and consent to participate

This research was approved by the Institutional Animal Care and Use Committee of PLA General Hospital.

CRediT authorship contribution statement

Liwei Fu: Writing – review & editing, Writing – original draft, Data curation, Conceptualization. **Jiang Wu:** Software, Data curation. **Pinxue Li:** Writing – original draft. **Yazhe Zheng:** Project administration, Methodology. **Zhichao Zhang:** Methodology, Investigation. **Xun Yuan:** Investigation. **Zhengang Ding:** Investigation. **Chao Ning:** Writing – review & editing, Writing – original draft. **Xiang Sui:** Writing – review & editing. **Shuyun Liu:** Writing – review & editing, Funding acquisition. **Sirong Shi:** Writing – review & editing. **Quanyi Guo:** Writing – review & editing, Funding acquisition. **Yunfeng Lin:** Writing – original draft.

Declaration of competing interest

The authors declare that they have no competing interests.

Acknowledgments

This study was supported by the Natural Science Foundation of Beijing Municipality (L234024). We thank Dr. Renwei Liu (Shimadzu) for help with the AFM measurements performed in this work.

Appendix A. Supplementary data

Supplementary data to this article can be found online at https://doi.org/10.1016/j.bioactmat.2024.08.008.

References

[1] H. Kwon, W.E. Brown, C.A. Lee, D. Wang, N. Paschos, J.C. Hu, K.A. Athanasiou, Surgical and tissue engineering strategies for articular cartilage and meniscus repair, Nat. Rev. Rheumatol. 15 (9) (2019) 550–570.
[2] A.R. Armiento, M. Alini, M.J. Stoddart, Articular fibrocartilage - why does hyaline cartilage fail to repair, Adv. Drug Deliv. Rev. 146 (2019) 289–305.
[3] D.J. Huey, J.C. Hu, K.A. Athanasiou, Unlike bone, cartilage regeneration remains elusive, Science 338 (6109) (2012) 917–921.
[4] R.F. Loeser, J.A. Collins, B.O. Diekman, Ageing and the pathogenesis of osteoarthritis, Nat. Rev. Rheumatol. 12 (7) (2016) 412–420.
[5] X. Guo, L. Xi, M. Yu, Z. Fan, W. Wang, A. Ju, Z. Liang, G. Zhou, W. Ren, Regeneration of articular cartilage defects: therapeutic strategies and perspectives, J. Tissue Eng. 14 (2023) 20417314231164765.
[6] R. Gilat, E.D. Haunschild, H.P. Huddleston, T.M. Tauro, S. Patel, T.S. Wolfson, K. C. Parvaresh, A.B. Yanke, B.J. Cole, Osteochondral allograft transplant for focal cartilage defects of the femoral condyles: clinically significant outcomes, failures, and survival at a minimum 5-year follow-up, Am. J. Sports Med. 49 (2) (2021) 467–475.
[7] T. Saris, T.S. de Windt, E.C. Kester, L.A. Vonk, R. Custers, D. Saris, Five-year outcome of 1-stage cell-based cartilage repair using recycled autologous chondrons and allogenic mesenchymal stromal cells: a first-in-human clinical trial, Am. J. Sports Med. 49 (4) (2021) 941–947.
[8] M. Jung, D.C. Karampinos, C. Holwein, J. Suchowierski, T.D. Diallo, A.S. Gersing, F. Bamberg, F.A. Baumann, S. Ruschke, P.M. Jungmann, Quantitative 3-T magnetic resonance imaging after matrix-associated autologous chondrocyte implantation with autologous bone grafting of the knee: the importance of subchondral bone parameters, Am. J. Sports Med. 49 (2) (2021) 476–486.
[9] S. Muthu, J.V. Korpershoek, E.J. Novais, G.F. Tawy, A.P. Hollander, I. Martin, Failure of cartilage regeneration: emerging hypotheses and related therapeutic strategies, Nat. Rev. Rheumatol. 19 (7) (2023) 403–416.
[10] C. Madeira, A. Santhagunam, J.B. Salgueiro, J.M. Cabral, Advanced cell therapies for articular cartilage regeneration, Trends Biotechnol. 33 (1) (2015) 35–42.
[11] B. You, C. Zhou, Y. Yang, MSC-EVs alleviate osteoarthritis by regulating microenvironmental cells in the articular cavity and maintaining cartilage matrix homeostasis, Ageing Res. Rev. 85 (2023) 101864.
[12] B.J. Huang, J.C. Hu, K.A. Athanasiou, Cell-based tissue engineering strategies used in the clinical repair of articular cartilage, Biomaterials 98 (2016) 1–22.
[13] T. Hoenig, K.E. Ackerman, B.R. Beck, M.L. Bouxsein, D.B. Burr, K. Hollander, K. L. Popp, T. Rolvien, A.S. Tenforde, S.J. Warden, Bone stress injuries, Nat. Rev. Dis. Prim. 8 (1) (2022) 26.
[14] Z. Yang, H. Li, Z. Yuan, L. Fu, S. Jiang, C. Gao, F. Wang, K. Zha, G. Tian, Z. Sun, B. Huang, F. Wei, F. Cao, X. Sui, J. Peng, S. Lu, W. Guo, S. Liu, Q. Guo, Endogenous cell recruitment strategy for articular cartilage regeneration, Acta Biomater. 114 (2020) 31–52.
[15] X.N. Xiang, S.Y. Zhu, H.C. He, X. Yu, Y. Xu, C.Q. He, Mesenchymal stromal cell-based therapy for cartilage regeneration in knee osteoarthritis, Stem Cell Res. Ther. 13 (1) (2022) 14.
[16] D. McGonagle, T.G. Baboolal, E. Jones, Native joint-resident mesenchymal stem cells for cartilage repair in osteoarthritis, Nat. Rev. Rheumatol. 13 (12) (2017) 719–730.
[17] S. Melnik, J. Gabler, S.I. Dreher, N. Hecht, N. Hofmann, T. Großner, W. Richter, MiR-218 affects hypertrophic differentiation of human mesenchymal stromal cells during chondrogenesis via targeting RUNX2, MEF2C, and COL10A1, Stem Cell Res. Ther. 11 (1) (2020) 532.
[18] C.C. Pritchard, H.H. Cheng, M. Tewari, MicroRNA profiling: approaches and considerations, Nat. Rev. Genet. 13 (5) (2012) 358–369.
[19] J. Krol, I. Loedige, W. Filipowicz, The widespread regulation of microRNA biogenesis, function and decay, Nat. Rev. Genet. 11 (9) (2010) 597–610.
[20] M.B. Goldring, K.B. Marcu, Epigenomic and microRNA-mediated regulation in cartilage development, homeostasis, and osteoarthritis, Trends Mol. Med. 18 (2) (2012) 109–118.
[21] M.R. Iaquinta, C. Lanzillotti, C. Mazziotta, I. Bononi, F. Frontini, E. Mazzoni, L. Oton-Gonzalez, J.C. Rotondo, E. Torreggiani, M. Tognon, F. Martini, The role of microRNAs in the osteogenic and chondrogenic differentiation of mesenchymal stem cells and bone pathologies, Theranostics 11 (13) (2021) 6573–6591.
[22] S. Yamashita, S. Miyaki, Y. Kato, S. Yokoyama, T. Sato, F. Barrionuevo, H. Akiyama, G. Scherer, S. Takada, H. Asahara, L-Sox5 and Sox6 proteins enhance chondrogenic miR-140 microRNA expression by strengthening dimeric Sox9 activity, J. Biol. Chem. 287 (26) (2012) 22206–22215.
[23] J.D. Kenyon, O. Sergeeva, R.A. Somoza, M. Li, A.I. Caplan, A.M. Khalil, Z. Lee, Analysis of -5p and -3p strands of miR-145 and miR-140 during mesenchymal stem cell chondrogenic differentiation, Tissue Eng. 25 (1–2) (2019) 80–90.
[24] M.E. Buechli, J. Lamarre, T.G. Koch, MicroRNA-140 expression during chondrogenic differentiation of equine cord blood-derived mesenchymal stromal cells, Stem Cell. Dev. 22 (8) (2013) 1288–1296.
[25] T.A. Karlsen, R.B. Jakobsen, T.S. Mikkelsen, J.E. Brinchmann, microRNA-140 targets RALA and regulates chondrogenic differentiation of human mesenchymal stem cells by translational enhancement of SOX9 and ACAN, Stem Cell. Dev. 23 (3) (2014) 290–304.
[26] R.L. Zhao, X.M. Zhang, L.N. Jia, W. Song, Y.L. Sun, X.Y. Meng, X.X. Peng, (p) NNS-conjugated chitosan mediated IGF-1 and miR-140 overexpression in articular chondrocytes improves cartilage repair, BioMed Res. Int. 2019 (2019) 2761241.
[27] K. Rajagopal, P. Arjunan, S. Marepally, V. Madhuri, Controlled differentiation of mesenchymal stem cells into hyaline cartilage in miR-140-activated collagen hydrogel, Cartilage 13 (2_suppl) (2021) 571S–581S.
[28] Z. Zhang, Y. Kang, Z. Zhang, H. Zhang, X. Duan, J. Liu, X. Li, W. Liao, Expression of microRNAs during chondrogenesis of human adipose-derived stem cells, Osteoarthritis Cartilage 20 (12) (2012) 1638–1646.
[29] Y. Ito, T. Matsuzaki, F. Ayabe, S. Mokuda, R. Kurimoto, T. Matsushima, Y. Tabata, M. Inotsume, H. Tsutsumi, L. Liu, M. Shinohara, Y. Tanaka, R. Nakamichi, K. Nishida, M.K. Lotz, H. Asahara, Both microRNA-455-5p and -3p repress hypoxia-inducible factor-2α expression and coordinately regulate cartilage homeostasis, Nat. Commun. 12 (1) (2021) 4148.
[30] Z. Zhang, C. Hou, F. Meng, X. Zhao, Z. Zhang, G. Huang, W. Chen, M. Fu, W. Liao, MiR-455-3p regulates early chondrogenic differentiation via inhibiting Runx2, FEBS Lett. 589 (23) (2015) 3671–3678.
[31] Y. Sun, J. Zhao, Q. Wu, Y. Zhang, Y. You, W. Jiang, K. Dai, Chondrogenic primed extracellular vesicles activate miR-455/SOX11/FOXO axis for cartilage regeneration and osteoarthritis treatment, NPJ Regen Med 7 (1) (2022) 53.
[32] T. Zhang, T. Tian, Y. Lin, Functionalizing framework nucleic-acid-based nanostructures for biomedical application, Adv. Mater. 34 (46) (2022) e2107820.
[33] Y. Lin, Q. Li, L. Wang, Q. Guo, S. Liu, S. Zhu, Y. Sun, Y. Fan, Y. Sun, H. Li, X. Tian, D. Luo, S. Shi, Advances in regenerative medicine applications of tetrahedral framework nucleic acid-based nanomaterials: an expert consensus recommendation, Int. J. Oral Sci. 14 (1) (2022) 51.
[34] W. Ma, X. Shao, D. Zhao, Q. Li, M. Liu, T. Zhou, X. Xie, C. Mao, Y. Zhang, Y. Lin, Self-assembled tetrahedral DNA nanostructures promote neural stem cell proliferation and neuronal differentiation, ACS Appl. Mater. Interfaces 10 (9) (2018) 7892–7900.
[35] S. Shi, Q. Peng, X. Shao, J. Xie, S. Lin, T. Zhang, Q. Li, X. Li, Y. Lin, Self-assembled tetrahedral DNA nanostructures promote adipose-derived stem cell migration via lncRNA XLOC 010623 and RHOA/ROCK2 signal pathway, ACS Appl. Mater. Interfaces 8 (30) (2016) 19353–19363.
[36] X.R. Shao, S.Y. Lin, Q. Peng, S.R. Shi, X.L. Li, T. Zhang, Y.F. Lin, Effect of tetrahedral DNA nanostructures on osteogenic differentiation of mesenchymal stem cells via activation of the Wnt/β-catenin signaling pathway, Nanomedicine 13 (5) (2017) 1809–1819.
[37] L. Fu, P. Li, J. Zhu, Z. Liao, C. Gao, H. Li, Z. Yang, T. Zhao, W. Chen, Y. Peng, F. Cao, C. Ning, X. Sui, Q. Guo, Y. Lin, S. Liu, Tetrahedral framework nucleic acids promote the biological functions and related mechanism of synovium-derived mesenchymal stem cells and show improved articular cartilage regeneration activity in situ, Bioact. Mater. 9 (2022) 411–427.
[38] X. Hu, Y. Wang, Y. Tan, J. Wang, H. Liu, Y. Wang, S. Yang, M. Shi, S. Zhao, Y. Zhang, Q. Yuan, A difunctional regeneration scaffold for knee repair based on aptamer-directed cell recruitment, Adv. Mater. 29 (15) (2017).
[39] Z. Hou, S. Meyer, N.E. Propson, J. Nie, P. Jiang, R. Stewart, J.A. Thomson, Characterization and target identification of a DNA aptamer that labels pluripotent stem cells, Cell Res. 25 (3) (2015) 390–393.
[40] T. Zhang, T. Tian, R. Zhou, S. Li, W. Ma, Y. Zhang, N. Liu, S. Shi, Q. Li, X. Xie, Y. Ge, M. Liu, Q. Zhang, S. Lin, X. Cai, Y. Lin, Design, fabrication and applications of tetrahedral DNA nanostructure-based multifunctional complexes in drug delivery and biomedical treatment, Nat. Protoc. 15 (8) (2020) 2728–2757.
[41] B.L. K Chen, W.Z. B Yu, Y. Lu, Advances in the Development of Aptamer Drug Conjugates for Targeted Drug Delivery, Wiley, 2017.
[42] K. Ghasemii, M. Darroudi, I. Rahimmanesh, M. Ghomi, M. Hassanpour, E. Sharifi, S. Yousefiasl, S. Ahmadi, A. Zarrabi, A. Borzacchiello, M. Rabiee, A.C. Paiva-Santos, N. Rabiee, Advances in aptamer-based drug delivery vehicles for cancer therapy, Biomater. Adv. 140 (2022) 213077.
[43] W. Alshaer, H. Hillaireau, E. Fattal, Aptamer-guided nanomedicines for anticancer drug delivery, Adv. Drug Deliv. Rev. 134 (2018) 122–137.
[44] M.R.D. N Rabiee, P.M. A Zarrabi, Green Biomaterials: Fundamental Principles, Biomaterials, 2023.
[45] Y. Jiang, S. Li, R. Shi, W. Yin, W. Lv, T. Tian, Y. Lin, A novel bioswitchable miRNA mimic delivery system: therapeutic strategies upgraded from tetrahedral framework nucleic acid system for fibrotic disease treatment and pyroptosis pathway inhibition, Adv. Sci. 11 (1) (2024) e2305622.
[46] Y. Yao, X. Lei, Y. Wang, G. Zhang, H. Huang, Y. Zhao, S. Shi, Y. Gao, X. Cai, S. Gao, Y. Lin, A mitochondrial nanoguard modulates redox homeostasis and bioenergy metabolism in diabetic peripheral neuropathy, ACS Nano 17 (22) (2023) 22334–22354.

[47] P. Li, L. Fu, Z. Liao, Y. Peng, C. Ning, C. Gao, D. Zhang, X. Sui, Y. Lin, S. Liu, C. Hao, Q. Guo, Chitosan hydrogel/3D-printed poly(ε-caprolactone) hybrid scaffold containing synovial mesenchymal stem cells for cartilage regeneration based on tetrahedral framework nucleic acid recruitment, Biomaterials 278 (2021) 121131.
[48] S. Zhang, B. Hu, W. Liu, P. Wang, X. Lv, S. Chen, H. Liu, Z. Shao, Articular cartilage regeneration: the role of endogenous mesenchymal stem/progenitor cell recruitment and migration, Semin. Arthritis Rheum. 50 (2) (2020) 198–208.
[49] L. Zhou, J. Xu, A. Schwab, W. Tong, J. Xu, L. Zheng, Y. Li, Z. Li, S. Xu, Z. Chen, L. Zou, X. Zhao, G. van Osch, C. Wen, L. Qin, Engineered biochemical cues of regenerative biomaterials to enhance endogenous stem/progenitor cells (ESPCs)-mediated articular cartilage repair, Bioact. Mater. 26 (2023) 490–512.
[50] J. Wei, D.T. Baptista-Hon, Z. Wang, G. Li, T. Herrler, C. Dai, K. Liu, B. Yu, X. Chen, M. Yang, D. Han, Y. Gao, R.L. Huang, L. Guo, K. Zhang, Q. Li, Bioengineered human tissue regeneration and repair using endogenous stem cells, Cell Reports Medicine 4 (8) (2023) 101156.
[51] Y.W. Z Li, X.L. C Zhao, Z.L. M Chen, J. Liu, Polysaccharide hybrid scaffold encapsulated endogenous factors for microfracture enhancement by sustainable release and cell recruitment, Composites, Part B (2024).
[52] T.F. Z Deng, H.T. C Xiao, C.L. Y Zheng, TGF-B Signaling in Health, Disease, and Therapeutics, … and Targeted Therapy, 2024.
[53] H.J. J Li, Z.S. Z Lv, G.T. C Cheng, M. Wang, Articular fibrocartilage-targeted therapy by microtubule stabilization, Science (2022).
[54] M.A. Ar Armiento, M.J. Stoddart, Articular fibrocartilage-Why does hyaline cartilage fail to repair, Adv. Drug Deliv. Rev. (2019).
[55] G. Pattappa, B. Johnstone, J. Zellner, D. Docheva, P. Angele, The importance of physioxia in mesenchymal stem cell chondrogenesis and the mechanisms controlling its response, Int. J. Mol. Sci. 20 (3) (2019) 484.
[56] N. van Gastel, S. Stegen, G. Eelen, S. Schoors, A. Carlier, V.W. Daniëls, N. Baryawno, D. Przybylski, M. Depypere, P.J. Stiers, D. Lambrechts, R. Van Looveren, S. Torrekens, A. Sharda, P. Agostinis, D. Lambrechts, F. Maes, J. V. Swinnen, L. Geris, H. Van Oosterwyck, B. Thienpont, P. Carmeliet, D.T. Scadden, G. Carmeliet, Lipid availability determines fate of skeletal progenitor cells via SOX9, Nature 579 (7797) (2020) 111–117.
[57] Y. Chen, W. Chen, Y. Ren, S. Li, M. Liu, J. Xing, Y. Han, Y. Chen, R. Tao, L. Guo, X. Sui, Q. Guo, S. Liu, Y. Han, Lipid nanoparticle-encapsulated VEGFa siRNA facilitates cartilage formation by suppressing angiogenesis, Int. J. Biol. Macromol. 221 (2022) 1313–1324.
[58] C.Y. Zeng, X.F. Wang, F.Z. Hua, HIF-1α in osteoarthritis: from pathogenesis to therapeutic implications, Front. Pharmacol. 13 (2022) 927126.
[59] X. Sun, H. Yin, Y. Wang, J. Lu, X. Shen, C. Lu, H. Tang, H. Meng, S. Yang, W. Yu, Y. Zhu, Q. Guo, A. Wang, W. Xu, S. Liu, S. Lu, X. Wang, J. Peng, In situ articular cartilage regeneration through endogenous reparative cell homing using a functional bone marrow-specific scaffolding system, ACS Appl. Mater. Interfaces 10 (45) (2018) 38715–38728.
[60] J. Wu, L. Fu, Z. Yan, Y. Yang, H. Yin, P. Li, X. Yuan, Z. Ding, T. Kang, Z. Tian, Z. Liao, G. Tian, C. Ning, Y. Li, X. Sui, M. Chen, S. Liu, Q. Guo, Hierarchical porous ECM scaffolds incorporating GDF-5 fabricated by cryogenic 3D printing to promote articular cartilage regeneration, Biomater. Res. 27 (1) (2023) 7.
[61] H. Madry, L. Gao, A. Rey-Rico, J.K. Venkatesan, K. Müller-Brandt, X. Cai, L. Goebel, G. Schmitt, S. Speicher-Mentges, D. Zurakowski, M.D. Menger, M.W. Laschke, M. Cucchiarini, Thermosensitive hydrogel based on PEO-PPO-PEO poloxamers for a controlled in situ release of recombinant adeno-associated viral vectors for effective gene therapy of cartilage defects, Adv. Mater. 32 (2) (2020) e1906508.
[62] G.M. Cunniffe, P.J. Díaz-Payno, E.J. Sheehy, S.E. Critchley, H.V. Almeida, P. Pitacco, S.F. Carroll, O.R. Mahon, A. Dunne, T.J. Levingstone, C.J. Moran, R. T. Brady, F.J. O'Brien, P. Brama, D.J. Kelly, Tissue-specific extracellular matrix scaffolds for the regeneration of spatially complex musculoskeletal tissues, Biomaterials 188 (2019) 63–73.
[63] J. Li, Y. Yao, Y. Wang, J. Xu, D. Zhao, M. Liu, S. Shi, Y. Lin, Modulation of the crosstalk between schwann cells and macrophages for nerve regeneration: a therapeutic strategy based on a multifunctional tetrahedral framework nucleic acids system, Adv. Mater. 34 (46) (2022) e2202513.
[64] T. Zhang, M. Zhou, D. Xiao, Z. Liu, Y. Jiang, M. Feng, Y. Lin, X. Cai, Myelosuppression alleviation and hematopoietic regeneration by tetrahedral-framework nucleic-acid nanostructures functionalized with osteogenic growth peptide, Adv. Sci. 9 (27) (2022) e2202058.